Spectrally resolved optical probing of laser induced magnetization dynamics in bismuth iron garnet

2016 J. Phys.: Condens. Matter 28 276002

(http://iopscience.iop.org/0953-8984/28/27/276002)

IOP Publishing Journal of Physics: Condensed Matter
J. Phys.: Condens. Matter **28** (2016) 276002 (7pp) doi:10.1088/0953-8984/28/27/276002

Spectrally resolved optical probing of laser induced magnetization dynamics in bismuth iron garnet

Benny Koene[1], Marwan Deb[2], Elena Popova[2], Niels Keller[2], Theo Rasing[1] and Andrei Kirilyuk[1]

[1] Radboud University Nijmegen, Institute for Molecules and Materials, Heyendaalseweg 135, 6525 AJ Nijmegen, The Netherlands
[2] GEMaC, CNRS-Université de Versailles St. Quentin en Yvelines, 45 avenue des Etats-Unis, 78035 Versailles Cedex, France

E-mail: b.koene@science.ru.nl

Received 18 January 2016, revised 5 May 2016
Accepted for publication 5 May 2016
Published 23 May 2016

Abstract
The spectrally resolved magnetization dynamics in bismuth iron garnet shows a fluence dependent light induced modification of the magneto-optical Faraday spectrum. It is demonstrated that the relative contributions from the tetrahedral and octahedral iron sites to the Faraday spectrum change due to the impact of the pump pulse. This change explains the observed deviation from a linear dependence of the amplitude of the oscillations on the fluence, as expected for the inverse Faraday effect.

Keywords: bismuth iron garnet, magnetisation dynamics, inverse Faraday effect

(Some figures may appear in colour only in the online journal)

1. Introduction

Studying the magnetization dynamics on the femtosecond time scale can reveal very useful information about the exchange interaction [1] that determines the time scale of the magnetization dynamics [2] in multi-sublattice anti-ferro- or ferri-magnets. To obtain knowledge about what happens on this time scale of the exchange interaction it is of primary importance to be able to probe the dynamics of the different sublattices independently.

Recently, for the multi-sublattice metallic magnetic alloy GdFeCo it was shown that the dynamics of the individual anti-ferromagnetically coupled elements can be measured with time-resolved x-ray magnetic circular dichroism (XMCD) [3]. Due to the element specific absorption resonances it was possible to observe an unexpected difference in the dynamics of the Fe and Gd spins. Later it was also shown that for specific materials a similar element specific sensitivity can be obtained with spectrally resolved optical pump probe measurements [4]. However for a material like bismuth iron garnet (BIG), the two ferrimagnetically coupled sublattices both consist of Fe, so it becomes very challenging, if not impossible to distinguish them by XMCD. The question is whether this could be done with optics. The magneto-optical spectrum is not determined by a single atom, but it is considerably influenced by interactions between neighboring atoms. It was suggested [5] that the spectral dependence of the Faraday rotation makes it possible to selectively probe the two anti-ferromagnetically coupled iron sites. This site specific probing would be possible in BIG as the spectral Faraday rotation caused by the two transitions located on the two different iron sites have only a minor spectral overlap.

Here we perform a spectral study of laser-induced magnetization dynamics in a ferrimagnetic BIG thin film. Although we do not observe any difference in dynamics between the two different iron sites, we do observe a pump induced change in the magneto-optical Faraday spectrum. This change is different for the parts in the spectrum that can be identified to originate from either one or the other iron sublattice. We show that with the observed change in the Faraday spectrum it can be explained that the amplitude of the oscillations excited by the inverse Faraday effect depends non-linearly on the pulse fluence.

This paper will start with a description of the sample and experimental setup in section 2. In section 3 the measured dynamics as a function of the probe wavelength is shown, followed by a study of the fluence dependence of the oscillations in section 4 while in section 5 the conclusions are given.

2. Sample and experimental setup

A 200 nm thick single crystalline and single phase BIG ($Bi_3Fe_5O_{12}$) film, grown epitaxially on a substituted $Gd_3Ga_5O_{12}(0\,0\,1)$ substrate by pulsed laser deposition [6], is investigated. BIG has a crystal structure that is similar to yttrium iron garnet, with bismuth replacing the yttrium atoms. Hence the bismuth atom is enclosed in a dodecahedral crystal structure formed by oxygen atoms while the iron atoms are enclosed in a tetrahedral (24 × in a unit cell) or octahedral (16 × in a unit cell) site [7, 8]. Like yttrium iron garnet, BIG is expected to have a magnetization of 5 μ_B (Bohr magneton) per formula unit, but experimentally only values up to 4.4 μ_B per formula unit are observed [9]. BIG is a ferrimagnet with an anti-ferromagnetic coupling between the tetrahedral and octahedral sites.

Among the iron garnets, BIG is known to have the largest magneto-optical response. It was shown before that the Faraday spectrum in bismuth substituted yttrium iron garnet, as well as for pure BIG, can be explained by electric dipole transitions originating from the tetrahedral and octahedral iron sites [5, 10, 11]. The enhanced magneto-optical effect in BIG as compared to yttrium iron garnet is considered to be a result of an increase in the spin–orbit splitting of the energy levels involved in the dipole transitions. This increase in the spin–orbit splitting is assigned to an interaction between the bismuth and iron atoms [12].

It is interesting to consider the Faraday spectrum of the current sample in more detail. For this reason in figure 1 the main result from [5] is shown where a very similar sample was studied. The figure shows the measured Faraday spectrum (open circles) together with fits to the data using a model based on two dipole transitions. The separate contributions from the tetrahedral and octahedral site are shown as well. By summing the contributions from the tetrahedral and octahedral iron site, the Faraday spectrum of BIG is obtained (Global Fit, black solid line). Due to the presence of absorption the sign of the Faraday spectrum is not easy to predict [13], however according to the model suggested by the authors of [5] the contribution from the tetrahedral site to the Faraday rotation is zero at a wavelength of about 460 nm, while the contribution from the octahedral site is close to a maximum at the same wavelength. At a wavelength of about 520 nm the contribution from the two iron sites is reversed. Now the contribution from the octahedral site is zero while the contribution from the tetrahedral site is close to its maximum. This means that by choosing the probe wavelength to be 460 or 520 nm we will be able to measure the magnetization dynamics in the octahedral, respectively tetrahedral iron site.

For the study of the dynamics we used an optical pump probe setup in transmission geometry. A Spectra Physics

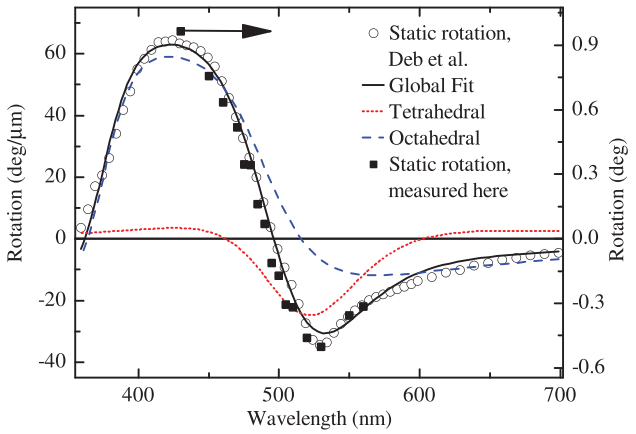

Figure 1. The Faraday spectrum of BIG as obtained by Deb *et al* [5] (solid line) and as measured here (black squares). The experimental data from Deb *et al* is supported by fits to the data using a model that treats the contributions from the tetrahedral and octahedral iron site separately. The seperate contributions from the tetrahedral and octahedral iron site to the global fit are shown respectively with a dotted and dashed line.

amplified laser system giving 40 fs, 800 nm pulses at a 1 kHz repetition rate was used as input for an optical parametric amplifier (OPA) and as the pump in the pump-probe scheme. The output of the OPA, which was varied between 430 and 560 nm, was used as the probe. A balanced photodetector combined with a lock-in amplifier was used for measuring the Faraday rotation, and an electromagnet supplied an in-plane magnetic field of 3 kOe.

The alignment of the pump beam was exactly perpendicular to the sample while the probe made an angle of about 10 deg with the sample normal. At this probe angle we are mainly sensitive to the out of plane magnetization while at the same time we can geometrically filter the pumplight out of the probe path. Measuring at different probe polarization angles did not show significant changes in the data which confirms that we are mainly sensitive to the out of plane magnetization component.

Depending on the measurement the spot size of the pump was 130 or 365 μm and that of the probe always about 26 μm. Other than in the measurements of the fluence dependence, the pump fluence was 27 mJ cm^{-2}. The probe pulse energy was at least 1000 × smaller than that of the pump. Here we only used circularly polarized light for the pump pulse, while the probe pulse polarization was linear.

To show that the sample discussed in this paper is similar to the one studied in [5], we have measured the static Faraday spectrum in the above explained experimental geometry by means of hysteresis loop measurements. The resulting data is compared in figure 1 (black squares) with that from Deb *et al* [5]. While here a longitudinal Faraday geometry with a very small tilt angle is used, in [5] a polar geometry was applied. Due to this difference in experimental geometry, the amplitude measured here is lower by a factor of 14. However, the spectral dependence is exactly the same.

Here we would like to note that besides *probing* at 460 and 520 nm, it could also be interesting to *pump* at those two wavelengths to separately address the two iron sites. Although an

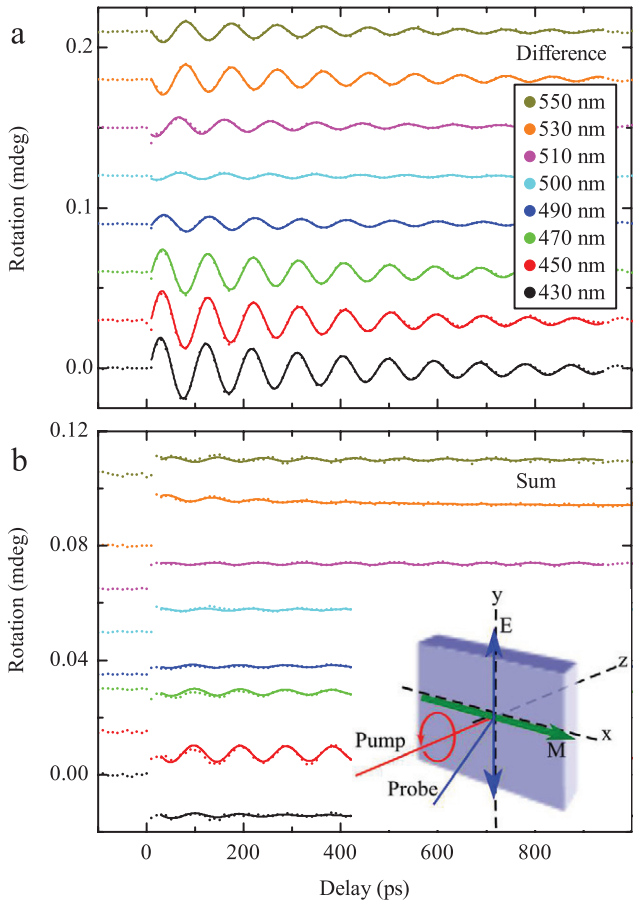

Figure 2. A selection of the magnetization dynamics measured at different probe wavelengths. In (a)/(b) the difference/sum of the measured dynamics with left and right circular polarization is shown. The solid lines are fits using equation (1). For better visibility the lines are offset from zero. The used offset for each line equals the rotation value of each line before zero delay. The inset represents a sketch of the experimental measurement configuration.

attempt was made with a pump at 400 nm, we could not reach similar high fluences as with an 800 nm pump in the experimental setup that was used. As the absorption at 400 nm is higher, this does not have to be a limitation. However, except in the oscillation amplitude we did not observe any other significant difference in the measured magnetization dynamics between using a 400 or 800 nm pump pulse.

3. Probe wavelength dependence

The dynamical response of the sample to excitation with both, left and right circularly polarized light is measured for a range of probe wavelengths. In figures 2(a) and (b), the measured dynamics is plotted as respectively the difference and the sum between the two polarization datasets. This data representation demonstrates that there is a polarization dependent (difference) as well as a polarization independent (sum) component present in the dynamical response of the sample.

The mechanism for the excitation of the magnetization precession in figure 2(a) is identified to be the inverse Faraday effect that gives rise to an effective optically induced magnetic field along the direction of the wave vector of the light; for more details see [14] and [15]. A clear disappearance of the oscillations is visible around 500 nm. Furthermore, the phase of the oscillations observed at wavelengths longer than 500 nm is shifted by π compared to the phase of the oscillations observed for a probe wavelength shorter than 500 nm. Alternatively one could state that the amplitude of the signal above 500 nm reverses sign. The latter statement is more in line with the known static Faraday rotation as shown in figure 1.

The sum signal in figure 2(b) shows, besides an offset in the rotation, oscillations as well. The origin of these oscillations, that are about one order of magnitude smaller compared to the polarization dependent oscillations, cannot be ascribed to the inverse Faraday effect, and is discussed in a separate paper [16]. Here we will thus focus on the wavelength dependence of the polarization dependent oscillations as well as the wavelength dependent offset that is visible in the polarization independent signal.

The measured magnetization dynamics is fitted with

$$y = y_0 + (B\mathrm{e}^{R_0 t}) + A\mathrm{e}^{-t/\tau}\sin(2\pi f t - \phi). \qquad (1)$$

Here y_0 is the offset, A is the amplitude of the oscillations, f is the frequency, τ is the oscillation lifetime, ϕ is the initial phase and t is the time. The term $B\mathrm{e}^{R_0 t}$ is only required to obtain a better fit i.e. a lower fitting error for a few curves (485 nm and 530 nm in the sum dataset and 495 nm in the fluence dependence dataset). Note that if the relaxation time ($1/R_0$) would be much larger compared to the scale of the graph, this term could interfere with the offset y_0. However, in the few cases it was used, this relaxation time was of the order of 400 ps. Although this is not negligible, it is only half the measured time range and the obtained fitting errors indicate a negligible dependency between y_0 and the second term in equation (1).

By fitting the difference dataset with equation (1) with the amplitude defined to be positive we obtain the phase versus wavelength dependence as shown in figure 3(a). The phase shift of π is clearly visible while going from 480 to 520 nm. In figure 3(b), the oscillation amplitude is shown for the difference dataset(red dots) as well as the static rotation data(black squares). Based on figure 3(a), the points measured at a wavelength of 500 nm or longer are represented as a negative value.

Other than the phase shift or sign change of the amplitude, the observed dynamics resulting from the tetrahedral and octahedral iron sites are identical. The decay time τ, which was a free fitting parameter as well, did not show a clear wavelength dependence and could be determined to be the same value of 450 ± 50 ps for all traces. Actually, on the time scale as shown in figure 2 an identical dynamics of the two sublattices is to be expected as the intersublattice exchange is strong enough to keep them aligned. Although we did perform measurements at shorter time scales as well, no distinct dynamics of the sublattices could be observed.

However, comparing in figure 3(b) the oscillation amplitude versus wavelength with the static Faraday spectrum we did observe a significant difference. The most obvious difference between the two curves is the wavelength at which a zero crossing occurs, i.e. the wavelength at which the two contributions from the tetrahedral and octahedral iron sites cancel

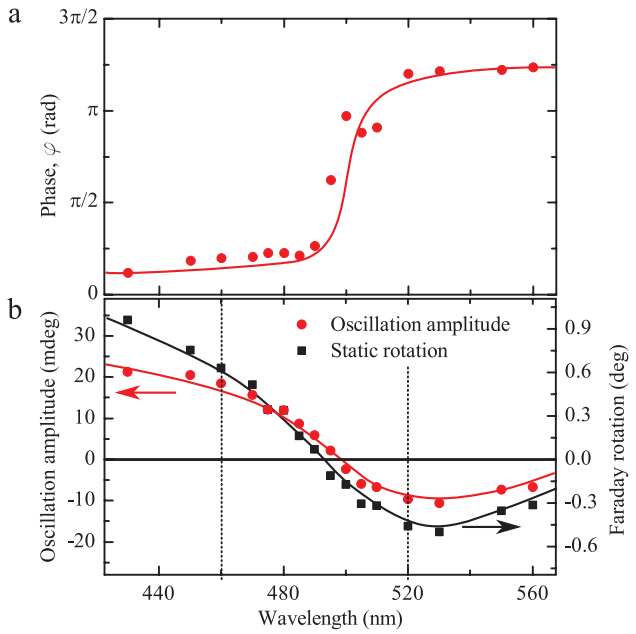

Figure 3. (a) The initial phase as obtained from a fit to the difference dataset with equation (1). A clear π phase change is observed at about 500 nm. The phase shift of π in (a) can also be represented as a change in the sign of the oscillation amplitude as is done in (b). For comparison the static spectral dependence of the hysteresis loop amplitude is given in (b) as well. A small shift of the zero crossing between static and dynamic spectral dependence is observed. The dashed lines indicate the wavelengths for which we expect to be sensitive to the octahedral or tetrahedral site only. The solid lines are guides to the eye.

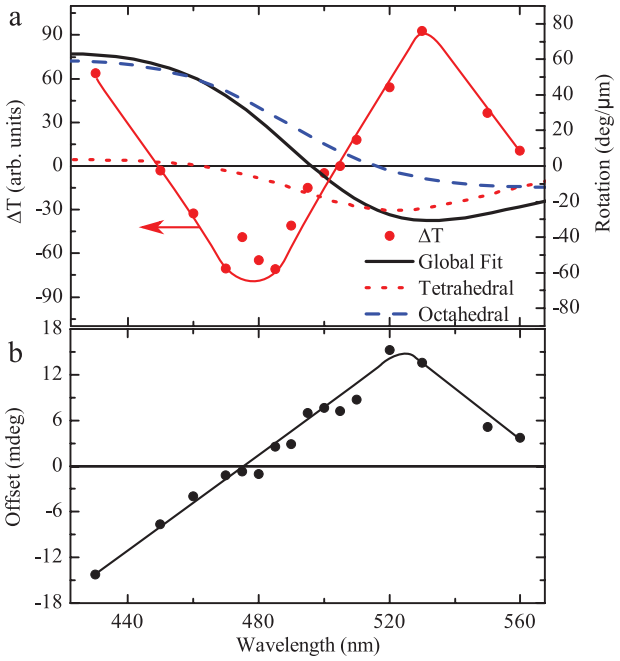

Figure 4. In (a) the pump induced change in transmission (ΔT) at a delay of 190 ps versus the probe wavelength is shown. The static spectral Faraday rotation, and the separate contributions from the two sublattices is also shown in the same graph. No correlation between the curves is found. In (b) the wavelength dependence of the offset y_0 is shown. This offset is obtained from fitting the data in figure 2(b) with equation (1). The solid line is a guide to the eye.

each other. For the dynamic measurements, this wavelength is red shifted by about 7 nm.

The uncertainty in wavelength in the data of figure 3 is related to the spectrum of the probe pulse from the OPA. This spectrum is about 5–10 nm broad. The static and dynamic measurements, however, are performed with exactly the same settings of the OPA, thus the data points at a single wavelength are directly comparable.

Although we do not have a definite answer about the mechanism behind this shift, we will suggest below that it can be explained by a pump induced change in the Faraday effect. This change in the Faraday effect most likely originates from a photo-induced change of the electronic structure such as state-filling or bleaching effects. Such a change might influence the dipole transitions that are responsible for the optical and magneto-optical constants. As the Faraday spectrum is formed by two different dipole transitions, it is possible that the spectral contributions from the two different iron sites to the Faraday rotation are changed in a different way.

Figure 4(a) shows the pump induced change in the intensity of the transmitted beam, demonstrating indeed a pump induced change in the optical constants. This pump induced change in transmission was measured in parallel with the measurement of the pump induced change in Faraday rotation. What is shown in figure 4(a) is the value of the transmission at a delay of 190 ps for the different probe wavelengths. It should be noted that the transmission data is not calibrated to take into account a difference in probe intensity or the spectral sensitivity of the detector.

The exact shape of the change in transmission curve is difficult to interpret. Together with the change in transmission, the static spectral Faraday rotation and the separate contributions from the two sublattices, is shown in figure 4(a) as well. Comparing the curves demonstrates the absence of any correlation between them.

Before we continue to discuss the observed pump induced spectral change in the Faraday rotation in figure 3(b), notice that there is no obvious connection between the amplitudes of the two curves shown in the figure. This gives the apparent freedom to scale the two curves relative to each other with a random scaling factor. However, the measured wavelength dependence of the offset y_0 determined from the sum dataset, will fix the choice of the scaling factor.

The offset, shown in figure 4(b), is a dc change in the observed Faraday rotation after the pump pulse hits the sample. The presence of an offset is clearly visible in the sum of the two measured helicities as shown in figure 2(b). A zero crossing of this offset occurs at a wavelength of about 475 nm. Thus at 475 nm the Faraday rotation before and after the pump pulse excites the sample remains the same. For this reason figure 3(b) is scaled such that the static spectrum of the Faraday rotation and the dynamic spectrum cross each other at the wavelength of 475 nm.

By using the scaling factor as defined in the above paragraph, the negative offset for wavelengths shorter than 475 nm agrees well with the decrease in Faraday rotation which can be observed in figure 3(b). The positive value of the offset for wavelengths longer than 475 nm agrees also with the increase

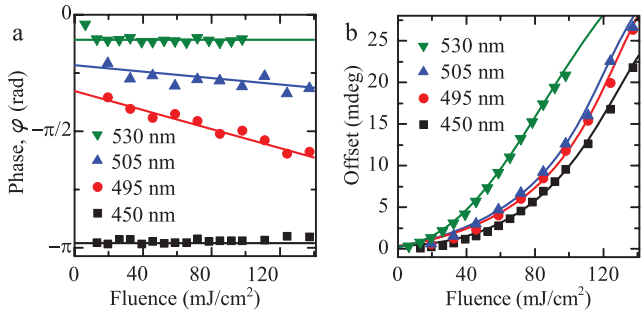

Figure 5. The initial phase (a) and absolute value of the offset (b) of the magnetization dynamics for four different probe wavelengths as a function of the pump fluence. The solid lines are guides to the eye.

in the Faraday rotation visible in this spectral region. Due to the negative sign of the Faraday rotation however, the absolute rotation might decrease.

Considering the data as shown in figure 3(b) the contribution from the tetrahedral site (520 nm) seems to be relatively stronger reduced as compared to the contribution from the octahedral site (460 nm). The absolute change is comparable for both sublattices. From figure 1, it is clear that if the relative contribution from the tetrahedral site is decreasing, the point for zero Faraday rotation red shifts. Hence a wavelength dependent difference in the relative change in the amplitude of the Faraday rotation originating from the two different iron sites seems to be responsible for the observed effect.

We would like to emphasize that the observed change in the Faraday rotation is not due to demagnetization, a process that is often observed in metallic magnetic materials [17, 18]. The change in Faraday rotation we measure here already reaches its maximum in the first measurement point after the pump illumination, hence in a time span of only a few picoseconds (see figure 2(b)). Demagnetization in dielectrics is not expected to occur on this time scale as the interaction between spins and phonons or electrons is known to be much slower [1].

4. Pump fluence dependence

In the previous section we ascribed the observed effect, i.e. the change in the spectral shape of Faraday rotation, to be pump induced. It is therefore interesting to measure the pump fluence dependence of the oscillations, in particular their amplitudes. We measured the fluence dependence of the magnetization dynamics at four different probe wavelengths. Especially the behavior of the initial phase, offset and the oscillation amplitude with increasing fluence will be discussed in this section. It should be noted that in this section only left circular polarized light is used. However from the measurements in the previous section we know that the observed dynamics is mainly determined by the inverse Faraday effect and the influence of the polarization independent oscillations shown in figure 2(b) can be ignored.

In figure 5(a), the fluence dependence of the initial phase is shown for four different wavelengths. Notice that the 450 and 530 nm are not the wavelengths of zero contribution from one or the other iron site. These wavelengths are chosen for experimental signal optimization. While the initial phase for a probe wavelength of 450 and 530 nm is constant with fluence, a decrease in the phase is visible for the other two wavelengths. As the latter wavelengths are close to the zero Faraday rotation point, the most straightforward explanation for this decrease in phase is a further shift of the zero rotation point to longer wavelengths. From figure 3(a), we know that when the zero rotation point is crossed, the phase will shift from 0 to π. Hence if this point is shifting further to the red then the phase shift will occur at longer wavelengths, and thus the initial phase at a wavelength around this zero point will show a decrease. In the investigated fluence region the initial phase continuously decreases for the wavelengths of 495 and 505 nm. This means that in the investigated fluence region the magneto-optical constants that describe the Faraday rotation spectrum change proportionally to the pump fluence.

A second indication for the modification with increasing pump power of the magneto-optical constants that describe the Faraday rotation spectrum is obtained from the offset dependence on the fluence as shown in figure 5(b). This value keeps on increasing for the fluences that are measured. Furthermore, from this figure, it is very clear that the rotation at 530 nm, which is mainly ascribed to the tetrahedral site, is changing much faster as compared to the rotation at 450 nm, which is assigned to the octahedral site. This thus confirms the earlier statement that the relative contribution from the tetrahedral site decreases more than the contribution from the octahedral site.

For garnets it is known that a two photon absorption processes exists at a wavelength of 800 nm, and thus might play a role in the effects we observe here. In figure 6(a), we show the fluence dependence of the transmission signal at a time delay of 190 ps. In the inset two typical time dependences of the transmission signal are shown. We are able to fit the fluence dependence data very well with $A + Bx^2$ suggesting the dominance of the two photon absorption process. The obtained fitting parameters are given in table 1.

Another important dependence to consider is the oscillation amplitude versus fluence which is shown in figure 6(b). We assigned the inverse Faraday effect as the starting mechanism for the magnetic precession. However, for the inverse Faraday effect in general a linear dependence of the oscillation amplitude A on the light fluence P, is expected. We will show below that with a fluence dependent Faraday rotation this does not have to be the case. In such a case A is given by:

$$A = \zeta P F(\lambda, P) d. \tag{2}$$

Here ζ is a scaling constant, $F(\lambda, P)$ the wavelength (λ) and fluence dependent Faraday rotation per unit distance, and d the sample thickness.

Although the amplitude depends approximately linear on the laser fluence up to 70 mJ cm^{-2}, above this value a clear deviation from the linear dependence is observed. This deviation can be explained by the variation in the magneto-optical constants with increasing fluence. As already indicated in equation (2), the Faraday rotation can be written as a function of the wavelength and the laser fluence. The wavelength

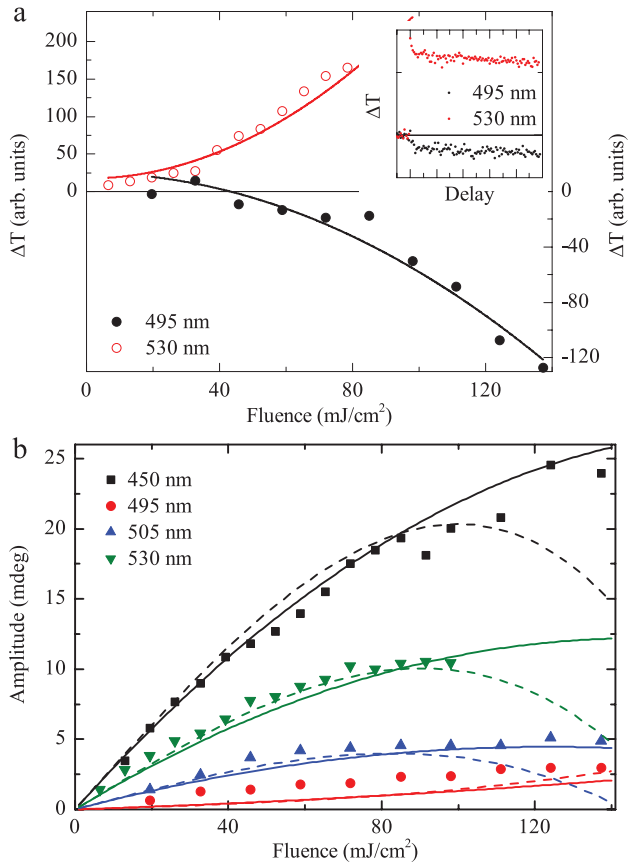

Figure 6. In (a) the change in transmission (ΔT) at a delay of 190 ps versus pump fluence is shown. The solid lines are fits to the data using $A + Bx^2$. The values for A and B can be found in table 1. In the inset two typical time dependencies of the change in transmission are given for a fluence of about 80 mJ cm^{-2}. The absolute value of the oscillation amplitude of the magnetization dynamics is shown in (b) for four different probe wavelengths as a function of the pump fluence. The measured data (symbols) is fitted with two models. One model (dashed lines) uses equations (2) and (3), while the other model (solid lines) uses equations (2) and (5). The used fitting parameters can be found in table 3.

dependence is given by the separate contributions from the two iron sites as shown in figure 1. We do not know the exact dependence of $F(\lambda, P)$ on the laser fluence P but a good first estimate is that it goes with the square of the fluence because we expect from figure 6(a) that the two photon absorption at 800 nm might play a role:

$$F = (1 - \eta P^2)F_t(\lambda) + (1 - \kappa P^2)F_o(\lambda). \quad (3)$$

Here η and κ are scaling constants that indicate the pump-induced decrease of the Faraday rotation for the tetrahedral and octahedral iron site, respectively. The static Faraday rotation from those sites are given by $F_t(\lambda)$ and $F_o(\lambda)$. The values of the last two functions for the four wavelengths shown in figure 6(b) are given in table 2. Equation (2) now can be written as:

$$A = \zeta dP[F_t(\lambda) + F_o(\lambda)] - \zeta dP^3[\eta F_t(\lambda) + \kappa F_o(\lambda)]. \quad (4)$$

As the scaling constants ζ, η and κ are assumed to be the same for all wavelengths, i.e. the optical pump only changes

Table 1. Resulting values for A and B when the fluence dependence of the transmission in figure 6(a) is fitted with $A + Bx^2$.

λ (nm)	A	$B, \times 10^{-2}$
495	13 ± 5	0.72 ± 0.06
530	17 ± 5	2.2 ± 0.1

Table 2. The Faraday rotation (deg μm^{-1}) used for $F_t(\lambda)$ and $F_o(\lambda)$ for the four wavelengths (nm) as shown in figure 6.

λ	$F_t(\lambda)$	$F_o(\lambda)$
450	2.315	54.217
495	−15.530	17.180
505	−20.940	7.554
530	−23.567	−7.244

Note: The values in this table are obtained from the curves indicated by tetrahedral and octahedral in figure 1.

Table 3. Resulting values for ζ, η and κ (cm^2 mJ^{-1}) from fitting the data in figure 6(b) at fixed fluence P (mJ cm^{-2}) with equation (2), using for the Faraday rotation F equation (3) (quadratic) or equation (5) (linear).

		Quadratic		Linear	
P	$\zeta, \times 10^{-6}$	$\eta, \times 10^{-4}$	$\kappa, \times 10^{-4}$	$\eta, \times 10^{-4}$	$\kappa, \times 10^{-4}$
19.6	27 ± 2	—	—	—	—
32.7	25 ± 2	—	—	—	—
85.0	27	43 ± 9	33 ± 5	36 ± 8	28 ± 5
98.0	27	41 ± 5	33 ± 3	40 ± 5	32 ± 3

Note: If no error is given this means that the value is fixed during the fitting. The '—' for η and κ represent that those variables are not taken into account.

the amplitude of the transitions $F_t(\lambda)$ and $F_o(\lambda)$, and not their spectral shape, we determined their approximate values by fitting the data points in figure 6(b) at a fixed fluence and variable wavelength. Unfortunately the three constants are not independent of each other. For this reason we first calculated an estimation for ζ at the lower fluences where the terms $(1 - \eta P^2)$ and $(1 - \kappa P^2)$ are still reasonably close to one. In a next step we calculated estimations for η and κ by performing a fit at the higher fluences using the already found estimation for ζ. The resulting values from this procedure are shown in table 3.

The values found for different fluences lie within the fitting error from each other and thus are reasonable values for this model. However using these values to plot the amplitude dependence on the fluence as is done by the dashed lines in figure 6(b), it is directly clear that the model fails to describe the experimental data accurately enough at high fluences.

Because of this mismatch at higher fluences we tried a linear dependence of F on the fluence as well. Physically this could mean a change of F due to single photon absorption. Thus instead of using equation (3) we used:

$$F = (1 - \eta P)F_t(\lambda) + (1 - \kappa P)F_o(\lambda). \quad (5)$$

The fitting parameters obtained with this model are shown as well in table 3. Again a two step fitting procedure is

employed. Furthermore the solid lines in figure 6(b) show that this model describes the data more accurate compared to the quadratic one.

The better match of the linear model suggests that the two photon absorption process alone cannot explain the observed phenomena. It thus remains unclear which phenomena exactly are responsible for the observed pump induced changes in the Faraday rotation. A combination of a linear and quadratic model might improve the match between data and fitted curve. However already now the fitting procedure has to be performed in two steps due to dependencies between the coefficients. We do thus not have enough data to perform a combined linear and quadratic fitting procedure.

Here we would like to emphasize that although an exact understanding of the underlying physical origin of the pump induced change in the Faraday rotation is still missing, the above models do show that the proposed dependence of the Faraday rotation on the laser fluence will lead to the observed nonlinear intensity dependence of the inverse Faraday effect.

In principle the oscillation amplitude could also decrease with increasing laser fluence due to heating of the sample by the laser pulses, which brings the sample temperature closer to the Curie temperature and thereby decreasing the Faraday rotation. However, the extinction coefficient for BIG at the used pump wavelength is very small, resulting in a low absorption. From the data and model as given in [5] we estimated that the temperature increase is below 1 K for the fluences as used here.

5. Conclusions

In this paper we have shown that the laser induced magnetization dynamics in bismuth iron garnet via the inverse Faraday effect depends non-linearly on the fluence. We have demonstrated that this is due to the fact that the relative contributions from the Faraday rotation of the tetrahedral and octahedral iron sites to the total Faraday spectrum change after excitation with a femtosecond laser pulse. The contribution from the tetrahedral site is stronger reduced by the pump pulse than the contribution from the octahedral iron site.

This results in a shift of the zero Faraday rotation point by about 7 nm to the red at a fluence of 27 $\mathrm{mJ\ cm^{-2}}$. By increasing the fluence the observed shift to the red increases further as is deduced from the phase, offset and amplitude dependence on the pump fluence. The observed change in Faraday rotation accounts for the non-linear dependence of the oscillation amplitude on the laser fluence.

The exact mechanism responsible for the change in the contribution from the two different iron sites remains unclear. We suggest it is related to a light induced change in the electronic structure of the material, e.g. by a state filling or bleaching effect, which on its turn influences the dipole transitions that are responsible for the magneto-optical properties of the sample.

Acknowledgments

We would like to thank A Toonen and A van Roij for technical support. This work was financially supported by de Nederlandse Organisatie voor Wetenschappelijk Onderzoek (NWO), de Stichting voor Fundamenteel Onderzoek der Materie (FOM) and the European Union via ERC grant agreement No 339813 (EXCHANGE).

References

[1] Kirilyuk A, Kimel A V and Rasing Th 2010 *Rev. Mod. Phys.* **82** 2731
[2] Kirilyuk A, Kimel A V and Rasing Th 2013 *Rep. Prog. Phys.* **76** 026501
[3] Radu I *et al* 2011 *Nature* **472** 205
[4] Khorsand A R, Savoini M, Kirilyuk A, Kimel A V, Tsukamoto A, Itoh A and Rasing Th 2013 *Phys. Rev. Lett.* **110** 107205
[5] Deb M, Popova E, Fouchet A and Keller N 2012 *J. Phys. D: Appl. Phys.* **45** 455001
[6] Popova E *et al* 2012 *J. Appl. Phys.* **112** 093910
[7] Gilleo M A and Geller S 1958 *Phys. Rev.* **110** 73
[8] Hansteen F 2006 Ultrafast optical control of magnetization in ferrimagnetic garnets *PhD Thesis* Radboud University Nijmegen
[9] Popova E, Galeano A F F, Deb M, Warot-Fonrose B, Kachkachi H, Gendron F, Ott F, Berini B and Keller N 2013 *J. Magn. Magn. Mater.* **335** 139
[10] Dionne G F and Allen G A 1993 *J. Appl. Phys.* **73** 6127
[11] Dionne G F and Allen G A 1994 *J. Appl. Phys.* **75** 6372
[12] Wittekoek S, Popma T J A, Robertson J M and Bongers P F 1975 *Phys. Rev.* B **12** 2777
[13] Zvezdin A K and Kotov V A 1997 *Modern Magnetoopticcs and Magnetooptical Materials* (Bristol: IOP)
[14] Kimel A V, Kirilyuk A, Usachev P A, Pisarev R V, Balbashov A M and Rasing Th 2005 *Nature* **435** 655
[15] Hansteen F, Kimel A, Kirilyuk A and Rasing Th 2005 *Phys. Rev. Lett.* **95** 047402
[16] Koene B, Deb M, Popova E, Keller N, Rasing T and Kirilyuk A 2015 *Phys. Rev.* B **91** 184415
[17] Beaurepaire E, Merle J-C, Daunois A and Bigot J-Y 1996 *Phys. Rev. Lett.* **76** 4250
[18] Koopmans B, van Kampen M, Kohlhepp J T and de Jonge W J M 2000 *Phys. Rev. Lett.* **85** 844